Determination of the Backbone Dihedral Angles φ in Human Ubiquitin from Reparametrized Empirical Karplus Equations

ARTICLE *in* JOURNAL OF THE AMERICAN CHEMICAL SOCIETY · MARCH 1996

Impact Factor: 12.11 · DOI: 10.1021/ja9535524

Determination of the Backbone Dihedral Angles ϕ in Human Ubiquitin from Reparametrized Empirical Karplus Equations

Andy C. Wang and Ad Bax*

Contribution from the Laboratory of Chemical Physics, National Institute of Diabetes and Digestive and Kidney Diseases, National Institutes of Health, Bethesda, Maryland 20892-0520

Received October 24, 1995[⊗]

Abstract: The backbone dihedral angle ϕ in polypeptides is characterized by four different *J* couplings: $^3J_{H^NH^\alpha}$, $^3J_{H^NC'}$, $^3J_{H^NC^\beta}$, and $^3J_{H^\alpha C'}$. E.COSY and quantitative *J* correlation techniques have been used to measure these couplings in the protein human ubiquitin, uniformly enriched in ^{13}C and ^{15}N. Assuming that the dihedral backbone angles in solution are identical to those in the X-ray structure of this protein and that H^N is located in the $C'-N-C^\alpha$ plane, Karplus relations for $^3J_{H^NH^\alpha}$, $^3J_{H^\alpha C'}$, and $^3J_{H^NC^\beta}$, have been reparametrized. The root-mean-square (rms) difference between measured values of $^3J_{H^NH^\alpha}$, $^3J_{H^\alpha C'}$, $^3J_{H^NC^\beta}$, and $^3J_{H^NC'}$ and their corresponding Karplus curves are 0.53, 0.25, 0.24, and 0.36 Hz, respectively, whereas the precision of these measurements is considerably better. For any given residue, the differences between the four measured *J* couplings and values predicted by their Karplus curves on the basis of the X-ray structure-derived ϕ angle are highly correlated with one another. On average, a root-mean-square change of 5.7° in the X-ray derived ϕ angles is needed to obtain optimal agreement with all four measured *J* couplings. There is no clear correlation between the ϕ angle correction needed and the out-of-plane position of the amide proton predicted by *ab initio* calculations. The small differences in ϕ angles therefore presumably result from small uncertainties in the atomic positions of the 1.8 Å X-ray structure. However, they may also be caused by genuine differences between the structure of the protein in solution and in the crystalline state or contain a contribution resulting from deviations from the assumption that the $H^N-N-C^\alpha-H^\alpha$ dihedral angle equals $\phi - 60°$.

The empirical relationship between three-bond *J* couplings, ^3J, and the intervening dihedral angle, established by Karplus,[1] plays an important role in studying molecular conformation using NMR spectroscopy. The Karplus equation relates ^3J to the intervening dihedral angle θ: $^3J = A\cos^2\theta + B\cos\theta + C$. The values of the Karplus parameters, *A*, *B*, and *C*, depend on the nuclei involved, and on their substituents.[2] Although the general validity of the Karplus relation is now well established, there has been no detailed study of the intrinsic accuracy of this empirical relationship when applied to the study of peptides and proteins and it has remained unclear to what extent it is influenced by effects such as bond strain, hydrogen bonding, electric field gradients, or remote substituents.

The present study focuses on the four couplings, $^3J_{H^NC'}$, $^3J_{H^NC^\beta}$, $^3J_{H^\alpha C'}$ and $^3J_{H^NH^\alpha}$, which are related to the dihedral backbone angle ϕ in polypeptides. Karplus equations for *J* couplings in peptides originally had been parametrized on a relatively small number of model compounds, which were either rigid or assumed to be freely rotating about the dihedral angle in question.[3−6] Conformationally constrained peptides and proteins for which high-resolution X-ray structures are available present a more direct opportunity for establishing the relationship between the size of the *J* coupling and the pertinent dihedral angle.[7−9] Particularly for small proteins which can be isotopically enriched with ^{13}C and ^{15}N, a variety of novel methods allows measurement of both homo- and heteronuclear *J* couplings with high precision.[10−28] The large number of calibration points available from a single spectrum on a single protein therefore allows for a far more detailed characterization

[⊗] Abstract published in *Advance ACS Abstracts,* February 15, 1996.

(1) Karplus, M. *J. Chem. Phys.* **1959**, *30*, 11−15.
(2) Altona, C.; Franke, R.; de Haan, R.; Ippel, J. H.; Daalmans, G. J.; Hoekzema, W. A. J. A.; van Wijk, J. *Magn. Reson. Chem.* **1994**, *32*, 670−678.
(3) Bystrov, V. F.; Portnova, S. L.; Tsetlin, V. I.; Ivanov, V. T.; Ovchinnikov, Y. A. *Tetrahedron* **1969**, *25*, 493−515.
(4) Bystrov, V. F. *Prog. NMR. Spectrosc.* **1976**, *10*, 41−81.
(5) Fischman, A. J.; Live, D. H.; Wyssbrod, H. R.; Agosta, W. C.; Cowburn, D. *J. Am. Chem. Soc.* **1980**, *102*, 2533−2539.
(6) Hansen, P. E.; Feeney, J.; Roberts, G. C. K. *J. Magn. Reson.* **1975**, *17*, 249−261.
(7) DeMarco, A.; Llinás, M.; Wüthrich, K. *Biopolymers* **1978**, *17*, 2727−2742.
(8) Pardi, A.; Billeter, M.; Wüthrich, K. *J. Mol. Biol.* **1984**, *180*, 741−751.
(9) Wang, A. C.; Bax, A. *J. Am. Chem. Soc.* **1995**, *117*, 1810−1813.
(10) Montelione, G. T.; Wagner, G. *J. Am. Chem. Soc.* **1989**, *111*, 5474−5475.
(11) Montelione, G. T.; Winkler, M. E.; Rauenbuehler, P.; Wagner, G. *J. Magn. Reson.* **1989**, *82*, 198−204.
(12) Wider, G.; Neri, D.; Otting, G.; Wüthrich, K. *J. Magn. Reson.* **1989**, *85*, 426−431.
(13) Sørensen, O. W. *J. Magn. Reson.* **1990**, *90*, 433−438.
(14) Delaglio, F.; Torchia, D. A.; Bax, A. *J. Biomol. NMR* **1991**, *1*, 439−446.
(15) Gemmecker, G.; Fesik, S. W. *J. Magn. Reson.* **1991**, *95*, 208−213.
(16) Ludvigsen, S.; Andersen, K. V.; Poulsen, F. M. *J. Mol. Biol.* **1991**, *217*, 731−736.
(17) Emerson, S. D.; Montelione, G. T. *J. Am. Chem. Soc.* **1992**, *114*, 354−356.
(18) Vuister, G. W.; Bax, A. *J. Biomol. NMR* **1992**, *2*, 401−405.
(19) Olsen, H. B.; Ludvigsen, S.; Sørensen, O. W. *J. Magn. Reson. Ser. A* **1993**, *104*, 226−230.
(20) Olsen, H. B.; Ludvigsen, S.; Sørensen, O. W. *J. Magn. Reson. Ser. A* **1993**, *105*, 321−322.
(21) Vuister, G. W.; Yamazaki, T.; Torchia, D. A.; Bax, A. *J. Biomol. NMR* **1993**, *3*, 297−306.
(22) Bax, A.; Vuister, G. W.; Grzesiek, S.; Delaglio, F.; Wang, A. C.; Tschudin, R.; Zhu, G. *Meth. Enzymol.* **1994**, *239*, 79−105.
(23) Biamonti, C.; Rios, C. B.; Lyons, B. A.; Montelione, G. T. *Adv. Biophys. Chem.* **1994**, *4*, 51−120.
(24) Seip, S.; Balbach, J.; Kessler, H. *J. Magn. Reson. Ser. B* **1994**, *104*, 172−179.
(25) Weisemann, R.; Rüterjans, H.; Schwalbe, H.; Schleucher, J.; Bermel, W.; Griesinger, C. *J. Biomol. NMR* **1994**, *4*, 231−240.
(26) Löhr, F.; Rüterjans, H. *J. Biomol. NMR* **1995**, *5*, 25−36.
(27) Schmidt, J. M.; Ernst, R. R.; Aimoto, S.; Kainosho, M. *J. Biomol. NMR* **1995**, *5*, 95−105.
(28) Eberstadt, M.; Gemmecker, G.; Mierke, D. F.; Kessler, H. *Angew. Chem., Int. Ed. Engl.* **1995**, *34*, 1671−1695.

0002-7863/96/1518-2483$12.00/0

of the Karplus relationship than could be obtained previously from the study of small model compounds.

Comparison of the experimental $^3J_{H^NH^\alpha}$ couplings in turkey lysozyme and those predicted from the Karplus relation using the corresponding dihedral angles ϕ, obtained from three X-ray structures solved at different atomic resolution (2.5, 2.2, and 1.5 Å), showed that the agreement between the measured and predicted *J* values improved with increasing resolution of the lysozyme structure, and also with decreasing values of the crystallographic *R* factor.[29] This result indicates that, at least for the lysozyme structures solved at 2.2 and 2.5 Å resolution, the uncertainty in the ϕ angle derived from the X-ray structure is a principal cause for the deviation between the measured and predicted $^3J_{H^NH^\alpha}$ values. This raises the question of whether it might be possible to determine the backbone ϕ angles in polypeptides with higher accuracy from NMR *J* couplings than from X-ray structures.

To address the above question, we have made careful and highly reproducible measurements of $^3J_{H^NC'}$, $^3J_{H^NC^\beta}$, $^3J_{H^\alpha C'}$, and $^3J_{H^NH^\alpha}$, all directly related to the ϕ angle, for most of the residues in the protein ubiquitin. The corresponding Karplus equations were reparametrized on the basis of these values and the corresponding X-ray structure-derived ϕ angles.[30] Assuming that the errors in the X-ray ϕ angles are small and random and that the ϕ angles are distributed over a sufficiently wide range of values, these errors, to first order, do not affect the parametrization of the Karplus relationship.

It will be shown that, for a given residue, deviations between the measured $^3J_{H^NC'}$, $^3J_{H^NC^\beta}$, $^3J_{H^\alpha C'}$, and $^3J_{H^NH^\alpha}$ values and those predicted from the Karplus equations are highly correlated with one another. This indicates that the deviations between the Karplus relation and the measured *J* values are indeed largely caused by small differences between the average ϕ angles prevailing in solution and those measured in the crystalline state and allows ϕ angles to be refined based on the NMR *J* couplings. Reparametrizations of the Karplus equations using these refined angles yield curves which, as expected, are very similar to the first set of Karplus curves for the common situation where ϕ angles are negative but show some differences in the sparsely populated positive ϕ region.

Experimental Section

Two samples of commercially obtained uniformly $^{13}C/^{15}N$ enriched human ubiquitin (VLI Research, Southeastern, PA) were used, 3.5 mg each in 220 μL Shigemi microcells (Shigemi Inc., Allison Park, PA), containing 30 mM sodium acetate buffer, pH 4.7. A sample dissolved in D_2O was used for the HCAN[C′]-E.COSY experiment and a sample dissolved in 95% H_2O, 5% D_2O for all other triple resonance experiments. In the nomenclature of E.COSY-type experiments, the passive spin to which *J* couplings are measured is enclosed by square brackets in the name of the experiment.[9] One sample of commercially obtained uniformly ^{15}N enriched human ubiquitin, 1.4 mM, pH 4.7, 10 mM NaCl, was used for the 3D HNHA quantitative *J* measurement[31] and the CT-HMQC *J*[32] experiments. Except for a quantitative HN(CO)HB *J* correlation spectrum, which was recorded on a Bruker DMX-500 spectrometer, all spectra were recorded on a Bruker AMX-600 spectrometer. All spectra were recorded at 30 °C. Both the DMX-500 and AMX-600 spectrometers were equipped with a triple resonance pulsed field gradient probehead and home-built gradient power supply units.

The HNCA[HA]-E.COSY spectrum for measurement of $^3J_{H^NH^\alpha}$ was recorded as a 32* × 24* × 512* (*n** denotes *n* complex points) 3D data matrix with acquisition times of 26.9 (t_1, ^{15}N), 10.1 (t_2, ^{13}C), and 106.5 ms (t_3, ^1H). The pulse sequence (Figure 1, supporting information) is analogous to the one originally proposed by Wagner et al.[33] but uses soft H^N pulses during the latter half of the pulse scheme.[23] The total measuring time was 20.6 h. Acquired data were apodized with a 59°-shifted squared sine-bell in the t_3 dimension, truncated at 1% ($\sin^2 175°$) at the end of the FID, with a 59°-shifted sine-bell in the t_2 dimension, truncated at 10% ($\sin 175°$), and with an untruncated squared 90°-shifted sine-bell in the t_1 dimension after extending the data with mirror-image linear prediction[34] (10 coefficients) to 64* points. Data were zero filled to yield a digital resolution of 18.6 (F_1), 18.6 (F_2), and 2.3 Hz (F_3).

A set of eight 2D constant-time (CT) HMQC *J* spectra[32] for measurement of $^3J_{H^NH^\alpha}$ was recorded using dephasing periods ($4T + 2\Delta$) of 45, 60, 80, 100, 120, 140, 170, and 200 ms. A composite $90_y°-200_x°-90_y°$ ^1H pulse was used instead of the regular 180° pulse in Figure 1 of ref 32. Improved inversion of the passive spin ($^1H^\alpha$) by this composite pulse results in a ~0.8% increase of the measured $^3J_{H^NH^\alpha}$ values over the use of the original scheme. The total recording time for the eight spectra was 20 h. The acquired data matrices contain 38*, 56*, 81*, 106*, 131*, 156*, 194*, and 231* complex points in the t_1 dimension. For all eight spectra mirror-image linear prediction (using 16 coefficients) was used to double the duration of the t_1 time domain, prior to apodization with a squared cosine-bell window function. All spectra were zero-filled to yield a digital resolution of 1.2 (F_1) and 4.5 Hz (F_2).

The water-flip-back version of the 3D HNHA experiment[31,32] for measurement of $^3J_{H^NH^\alpha}$ was recorded as a 47* × 70* × 512* 3D data matrix with acquisition times of 38.2 (t_1, ^{15}N), 15.4 (t_2, ^1H), and 55.3 ms (t_3, ^1H). The total acquisition time was 44 h. Acquired data were apodized with a 65°-shifted squared sine-bell in the t_3 dimension, truncated at 10% (at $\sin^2 162°$) at the end of the FID, and with a 68°-shifted sine-bell in the t_2 dimension, truncated at 16% ($\sin 171°$). The t_1 (^{15}N) time domain data were extended to 83* data points by mirror-image linear prediction, prior to apodization with a squared 90°-shifted sine-bell and zero filling to 128*. Data were zero filled to yield a digital resolution of 9.6 (F_1), 17.8 (F_2), and 4.5 Hz (F_3).

The HCAN[C′]-E.COSY experiment (Figure 2, supporting information) for measurement of $^3J_{H^\alpha C'}$ was recorded as a 48* × 130* × 384* 3D data matrix with acquisition times of 28.5 (t_1, ^{13}C), 98.8 (t_2, ^{15}N), and 79.9 ms (t_3, ^1H). The total acquisition time was 28.8 h. Acquired data were apodized with a 72°-shifted squared sine-bell in the t_3 dimension, truncated at 1%, with a 59°-shifted sine-bell in the t_2 dimension, truncated at 10%, and with a 72°-shifted sine-bell in the t_1 dimension, truncated at 6%. Data were zero filled to yield a digital resolution of 13.2 (F_1), 2.6 (F_2), and 2.3 Hz (F_3).

The HN(CO)HB 3D spectrum[35] for measurement of $^3J_{H^\alpha C'}$ was recorded as a 35* × 70* × 1024* 3D data matrix with acquisition times of 26.6 (t_1, ^{15}N), 13.7 (t_2, ^1H), and 114.0 ms (t_3, ^1H) on a Bruker DMX-500 spectrometer (Figure 3, supporting information) using an improved version which uses shaped composite pulse decoupling on the $^{13}C^\alpha$ spins[25,36] during ^{15}N evolution and $^1H^{\alpha/\beta}$ evolution. Hardware limitations prevented use of the new pulse sequence on our AMX-600 spectrometer. The total acquisition time was 93.1 h. A 2D reference spectrum (35* × 1024*) was recorded using the same pulse scheme but an alternate phase cycling scheme, as indicated in the legend to Figure 3 in the supporting information. The total acquisition time for the 2D reference spectrum was 42 min. In addition, a 3D data matrix was recorded with the conventional scheme[22] on a Bruker AMX-600. For both data sets, acquired data were apodized with a 59°-shifted squared sine-bell in the t_3 dimension, truncated at 1%, with a cosine-bell in the t_2 dimension, truncated at 6%, and with an untruncated squared cosine-bell in the t_1 dimension after mirror-image linear

(29) Bartik, K.; Dobson, C. M.; Redfield, C. *Eur. J. Biochem.* **1993**, *215*, 255−266.
(30) Vijay-Kumar, S.; Bugg, C. E.; Cook, W. J. *J. Mol. Biol.* **1987**, *194*, 531−544.
(31) Vuister, G. W.; Bax, A. *J. Am. Chem. Soc.* **1993**, *115*, 7772−7777.
(32) Kuboniwa, H.; Grzesiek, S.; Delaglio, F.; Bax, A. *J. Biomol. NMR* **1994**, *4*, 871−878.
(33) Wagner, G.; Schmieder, P.; Thanabal, V. *J. Magn. Reson.* **1991**, *93*, 436−440.
(34) Zhu, G.; Bax, A. *J. Magn. Reson.* **1992**, *100*, 202−207.
(35) Grzesiek, S. G.; Ikura, M.; Clore, G. M.; Gronenborn, A. M.; Bax, A. *J. Magn. Reson.* **1992**, *96*, 215−221.
(36) McCoy, M. A.; Mueller, L. *J. Magn. Reson. Ser. A* **1993**, *101*, 122−130.

prediction (12 coefficients) was used to extend the data to 70* points. Data were zero filled to yield a digital resolution of 5.1 (F_1), 19.9 (F_2), and 4.4 Hz (F_3).

The HNCA[CB]-E.COSY experiment for measurement of $^3J_{H^NC^\beta}$ (Figure 4, supporting information) was recorded as a 32* × 56* × 768* 3D data matrix with acquisition times of 26.9 (t_1, ^{15}N), 40.3 (t_2, ^{13}C), and 98.3 ms (t_3, ^{1}H). Total acquisition time was 38.4 h. Note that the spectral width in the F_2 ($^{13}C^\alpha$) dimension was only 9.2 ppm, resulting in extensive aliasing in this dimension of the 3D spectrum. Acquired data were apodized with a 65°-shifted squared sine-bell in the t_3 dimension, truncated at 1%, with a 54°-shifted sine-bell in the t_2 dimension, truncated at 10%, and with an untruncated squared cosine-bell in the t_1 dimension after mirror-image linear prediction (10 coefficients) was used to extend the data to 64* points. Data were zero filled to yield a digital resolution of 9.2 (F_1), 4.6 (F_2), and 3.8 Hz (F_3).

Data collection and processing of the 3D HNCA[C′]-E.COSY spectrum are described elsewhere[9] and the $^3J_{H^NC'}$ data used in the present work were taken from that study.

Resonance assignments follow those reported previously.[37] Data were processed using the package NMRPipe[38a] and peak positions for all E.COSY- type spectra were determined with the program CAPP.[38b] The peak positions were found to be most reproducible between duplicate data sets when they were determined by fitting ellipsoids to each of the calculated contours between 60 and 80% of the peak maximum. The center of each ellipsoid provides a measure for the peak position and values obtained for all contours in the 60−80% intensity range of a given peak were averaged to provide the peak position used in the E.COSY-type J measurement. This procedure for peak position determination improved the reproducibility of the J couplings measured in consecutive experiments by approximately a factor of 2 relative to conventional peak picking algorithms. Peak positions and intensities for experiments that are not of the E.COSY type were determined interactively using common polynomial interpolation with the program PIPP.[38b]

Results

Four different types of J couplings, all related to the backbone ϕ angle, have been measured for most of the 76 residues in human ubiquitin. All experiments were performed at least twice and the pairwise deviation between J values provides an estimate for the precision of the measurements. Furthermore, for all but the $^3J_{H^NC^\beta}$ coupling, both E.COSY[23,28,39] and quantitative J correlation schemes[22] were used. Possible systematic errors in these different types of measurements are likely to be different and therefore can be estimated from the pairwise difference between measured J values.

Measurement of $^3J_{H^NH^\alpha}$. $^3J_{H^NH^\alpha}$ values were measured using three different techniques: The triple resonance HNCA[HA]-E.COSY experiment,[33] the 3D ^{15}N-separated HNHA experiment,[31,32] and a J-modulated 2D experiment.[32] The 3D HNCA-[HA]-E.COSY pulse sequence (Figure 1, supporting information) contains several minor modifications relative to the original scheme, including the use of pulsed field gradients[40] and selective H^N pulses. The Bruker AMX code for this pulse sequence is available as supporting information and will be deposited at the BioMagResBank (Madison, WI).

In the HNCA[HA]-E.COSY spectrum, the H^N resonance is correlated with its intraresidue C$^\alpha$. As no ^{1}H$^\alpha$ decoupling is used during ^{13}C$^\alpha$ evolution, the ^{13}C$^\alpha$ nucleus shows two resonances in the F_2 dimension, separated by $^1J_{H^\alpha C^\alpha}$ and corresponding to the $^1H^\alpha = |\alpha\rangle$ and $^1H^\alpha = |\beta\rangle$ spin states. Provided that the ^{1}H$^\alpha$ nucleus does not alter its spin state between ^{13}C$^\alpha$ evolution and ^{1}H^N detection, the relative displacement of these two resonances in the F_3 dimension corresponds to $^3J_{H^NH^\alpha}$. If a fraction of the ^{1}H$^\alpha$ nuclei changes their spin state between ^{13}C$^\alpha$ evolution and ^{1}H^N detection, the line shape of the detected amide proton, correlated with one of the two ^{13}C$^\alpha$ doublet lines, is altered from a singlet into an unresolved and asymmetric doublet (inset in Figure 1A). The finite lifetime of the spin state of the passive spin therefore results in an underestimate of $^3J_{H^NH^\alpha}$. Thus, selective ^{1}H^N pulses[23] are preferred over a non-selective 90°(^{1}H)−τ−180°(^{1}H,^{15}N)−τ−90°(^{1}H) bilinear pulse combination in the final reverse INEPT part of the sequence[13,24−26] as rapid transverse relaxation of ^{1}H$^\alpha$−{^{13}C$^\alpha$} magnetization during the τ delays (*ca.* 2.5 ms each) of the bilinear pulse only partially restores the H$^\alpha$ spin state after the bilinear pulse.

Görlach et al.[41] have presented an elegant variation of the HNCA[HA]-E.COSY pulse scheme which creates multiple quantum coherence between ^{15}N and ^{1}H^N and thereby removes the effect of ^{1}H$^\alpha$−^{1}H^N spin flips from the selective ^{1}H$^\alpha$ longitudinal relaxation time, $T_{1\alpha}$. However, as noted by Görlach et al., this is achieved at a cost in sensitivity, and this version of the E.COSY experiment has not been used in our study of ubiquitin.

Figure 1A shows F_1 strips taken from the 3D HNCA[HA]-E.COSY spectrum for residues Leu[43], Ile[44], Phe[45], and Ala[46]. Each of the amides has an intense correlation to its intraresidue C$^\alpha$−{H$^\alpha$} doublet and a weaker one to the C$^\alpha$−{H$^\alpha$} doublet of the preceding residue. This latter doublet results from magnetization transfer via $^2J_{NC^\alpha}$.[33,42] The relative horizontal displacement of the intraresidue C$^\alpha$-{H$^\alpha$} doublet components provides a measure for $^3J_{H^NH^\alpha}$. The displacement of the C$^\alpha$-

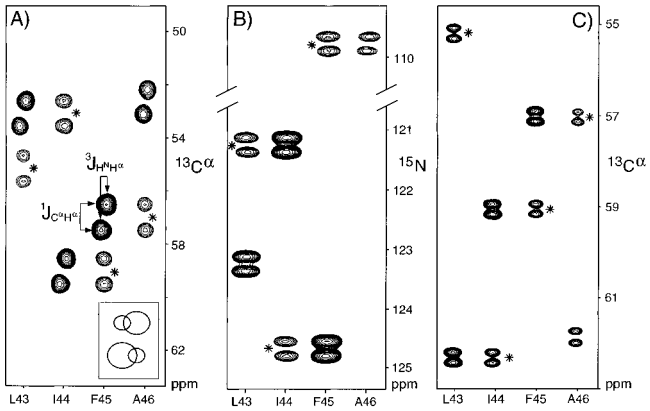

Figure 1. F_1 strips taken from (F_1,F_3) planes of (A) the HNCA[HA]-E.COSY, (B) the HCAN[C′]-E.COSY, and (C) the HNCA[CB]-E.COSY spectra for residues Leu[43]−Ala[46]. Asterisks mark the sequential H^N(i)−C$^\alpha$(i − 1) correlations which are of no interest in the present analysis of three-bond J couplings. Owing to the narrow ^{13}C$^\alpha$ spectral width used in the HNCA[CB]-E.COSY experiment (9.2 ppm), extensive aliasing of ^{13}C$^\alpha$ resonances has occurred relative to panel A. The inset in part A shows the result of passive spin flips on the E.COSY in-phase multiplet: Besides the two main doublet components (large ellipsoids) which are separated by $^3J_{H^NH^\alpha}$ in the horizontal dimension, smaller components result from a change in H$^\alpha$ spin state between ^{13}C$^\alpha$ evolution and ^{1}H^N detection. The small components are generally not resolvable, but result in an apparent shift of the adjacent larger components and thereby in a reduction of the measured splitting.

(37) (a) Di Stefano, D. L; Wand, A. J. *Biochemistry* **1987**, *26*, 7272−7281. (b) Weber, P. L.; Brown, S. C.; Mueller, L. *Biochemistry* **1987**, *26*, 7282−7290. (c) Schneider, D. M.; Dellwo, M. J.; Wand, A. J. *Biochemistry* **1992**, *31*, 3645−3652. (d) Wang, A. C.; Grzesiek, S.; Tschudin, R.; Lodi, P. J.; Bax, A. *J. Biomol. NMR* **1995**, *5*, 376−382.

(38) (a) Delaglio, F.; Grzesiek, S.; Vuister, G. W.; Zhu, G.; Pfeifer, J.; Bax, A. *J. Biomol. NMR* In press. (b) Garrett, D. S.; Powers, R.; Gronenborn, A. M.; Clore, G. M. *J. Magn. Reson.* **1991**, *95*, 214−220.

(39) Griesinger, C.; Sørensen, O. W.; Ernst, R. R. *J. Am. Chem. Soc.* **1985**, *107*, 6394−6396.

(40) Bax, A.; Pochapsky, S. S. *J. Magn. Reson.* **1992**, *99*, 638−643.

(41) Görlach, M.; Wittekind, M.; Farmer, B. T., II; Kay, L. E.; Mueller, L. *J. Magn. Reson.* **1993**, *101*, 194−197.

(42) Ikura, M.; Kay, L. E.; Bax, A. *Biochemistry* **1990**, *29*, 4659−4667.

{H^α} doublet components of the preceding residue corresponds to $^4J_{H^NH^\alpha}$, which for most common backbone conformations is very small.[43] The finite lifetime of the H^α spin state visibly distorts the peak shapes of the two doublet components, as shown schematically in the inset of Figure 1A. The magnitude of the correction for $^3J_{H^NH^\alpha}$ can be estimated if its selective $^1H^\alpha$ longitudinal relaxation rate, $R_{1\alpha} \equiv T_{1\alpha}^{-1}$, is known. Measured $R_{1\alpha}$ values in ubiquitin, using scheme 2f of Peng and Wagner[44] modified to measure the selective T_1 of ^{13}C- instead of ^{15}N-attached protons, average 4.6 ± 1.2 s^{-1} (Table 1, supporting information). Multiplet simulations (Figure 5, supporting information), based on a $R_{1\alpha}$ of 4.6 s^{-1} and the use of identical data processing and peak picking procedures as were used for the experimental data, indicate that $^3J_{H^NH^\alpha}$ couplings of, for example, 4, 7, and 10 Hz will be measured as splittings of 3.1, 5.9, and 9.2 Hz, respectively. Note, however, that the difference between the apparent splitting and the true *J* coupling depends on the way the peak postion is determined. The dashed line in Figure 2A illustrates the relation between the true $^3J_{H^NH^\alpha}$ coupling and the splitting measured from the simulated data, when peak picking is performed in the manner described in the Experimental Section. This curve was used to correct the $^3J_{H^NH^\alpha}$ couplings measured from the experimental spectrum. Note that the equation which relates the apparent splitting in a 1D spectrum to the true *J* coupling[45] yields different results as this equation does not apply to E.COSY-type patterns. Moreover, this equation does not account for spin flips of the H^α spins that occur between C^α evolution and H^N detection.

For small and rapidly tumbling proteins such as ubiquitin (M_r = 8565) a second and very precise method for measuring $^3J_{H^NH^\alpha}$ relies on fitting the damped oscillation of $^1H-^{15}N$ correlation intensities in a set of 2D *J*-modulated constant-time HMQC spectra,[32] collected using schemes analogous to those proposed by Neri et al.[46] and Billeter et al.[47] In the CT-HMQC *J* experiment, the intensity, *I*, of a correlation is given as a function of the total dephasing time, *t*, by[32]

$$I(t) = I(0)N_1 \exp[-t/T_{2,MQ} - T/(2T_{1\alpha})]\{\cos(\pi J^r t) + \sin(\pi J^r t)/(2\pi J^r T_{1\alpha})\} \quad (1a)$$

with

$$J^r = [(^3J_{H^NH\alpha})^2 - 1/(2\pi T_{1\alpha})^2]^{1/2} \quad (1b)$$

where N_1 is the number of t_1 increments in the 2D experiment and $T_{2,MQ}$ is the relaxation time of the $^1H-^{15}N$ multiple quantum coherence. As can be seen from eq 1b, the apparent modulation frequency, J^r, is reduced as a result of the finite $T_{1\alpha}$ values. Figure 3 shows best fits of eq 1 to the *J*-modulated CT-HMQC peak heights for the $^1H^N-^{15}N$ correlations of residues Leu[43]–Ala[46], as a function of the total dephasing time. $^3J_{H^NH^\alpha}$ values measured from two sets of *J*-modulated CT-HMQC spectra, both recorded at 30 °C, show a pairwise rms difference of only 0.028 Hz, indicating a random error of only 0.014 Hz in their averaged values. The principal sources of uncertainty therefore stem from possible systematic errors and from the uncertainty in the value of $R_{1\alpha}$. Measured $R_{1\alpha}$ values in duplicate relaxation experiments indicate a random uncertainty in $R_{1\alpha}$ of 0.1 s^{-1} and its effect on $^3J_{H^NH^\alpha}$, calculated from eq 1, therefore should be extremely small. Even using a $R_{1\alpha}$ off by 2 s^{-1} in eq 1 causes less than a 0.1-Hz change in $^3J_{H^NH^\alpha}$ values that are larger than 3 Hz (Figure 6, supporting information).

$^3J_{H^NH^\alpha}$ values have also been measured using the 3D HNHA experiment,[31,32] which is primarily intended for proteins which are too large for the *J*-modulated CT-HMQC method. The values agree well with those measured from the CT-HMQC

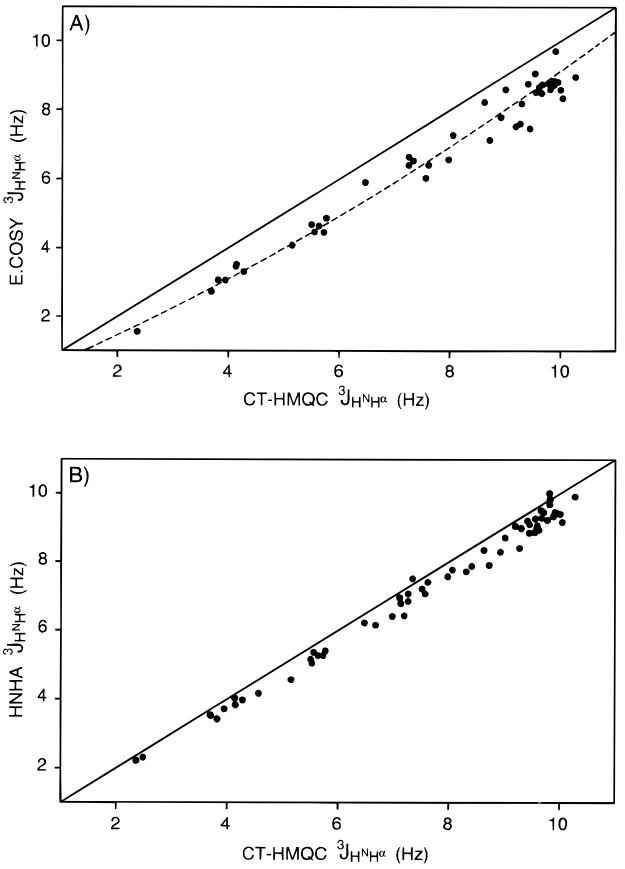

Figure 2. Plots of CT-HMQC-derived $^3J_{H^NH^\alpha}$ values *versus* (A) HNCA-[HA]-E.COSY-derived $^3J_{H^NH^\alpha}$ splittings and (B) $T_{1\alpha}$-corrected 3D HNHA-derived $^3J_{H^NH^\alpha}$. The lines in part A indicate the relation between $^3J_{H^NH^\alpha}$ splittings measured from simulated spectra (Figure 5, supporting information), using $T_{1\alpha}$ = 217 ms (dashed line) and $T_{1\alpha} = \infty$ (solid line). In part B, the solid line represents $y = x$, and HNHA-derived $^3J_{H^NH^\alpha}$ values are systematically about 0.4 Hz smaller than those derived from CT-HMQC.

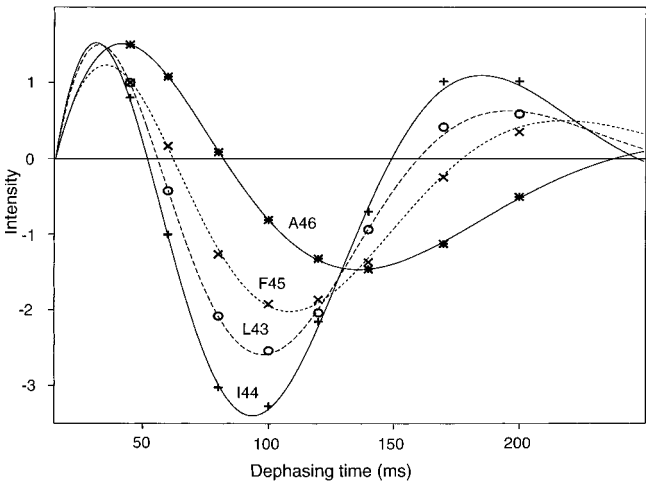

Figure 3. Best fits of eq 1 to the peak heights of residues Leu[43]–Ala[46] as a function of the dephasing time of the eight *J*-modulated CT-HMQC spectra.

(43) Vuister, G. W.; Bax, A. *J. Biomol. NMR* **1994**, *4*, 193–200.
(44) Peng, J. W.; Wagner, G. *J. Magn. Reson.* **1992**, *98*, 308–332.
(45) Harbison, G. S. *J. Am. Chem. Soc.* **1993**, *115*, 3026–3027.
(46) Neri, D.; Otting, G.; Wüthrich, K. *J. Am. Chem. Soc.* **1990**, *112*, 3663–3665.
(47) Billeter, M.; Neri, D.; Otting, G.; Qian, Y. Q.; Wüthrich, K. *J. Biomol. NMR* **1992**, *2*, 257–274.

Table 1. Coefficients[a] of Karplus Equations, $J = A\cos^2(\phi + \theta) + B\cos(\phi + \theta) + C$

	θ	A	B	C	ϕ
$^3J_{H^NH^\alpha}$	−60°	+6.64 (0.11)[b]	−1.43 (0.04)[b]	+1.86 (0.09)[b]	X-ray[c]
	−60°	+6.98 (0.04)	−1.38 (0.04)	+1.72 (0.03)	NMR/X-ray[d]
$^3J_{H^\alpha C'}$	−60°	+3.62 (0.07)	+2.11 (0.08)	+1.29 (0.04)	X-ray
	−60°	+3.75 (0.05)	+2.19 (0.06)	+1.28 (0.03)	NMR/X-ray
$^3J_{H^NC^\beta}$	+60°	+2.78 (0.07)	−0.37 (0.04)	+0.03 (0.03)	X-ray
	+60°	+3.39 (0.07)	−0.94 (0.08)	+0.07 (0.03)	NMR/X-ray
$^3J_{H^NC'}$	0°	+4.02 (0.14)	+1.12 (0.06)	+0.07 (0.02)	X-ray
	0°	+4.32 (0.08)	+0.84 (0.03)	+0.00 (0.02)	NMR/X-ray

[a] Karplus coefficients determined from singular value decomposition analysis. [b] Uncertainties in the coefficients, shown in parentheses, were calculated from 1000 fits of the data, omitting 10% of the data points, randomly chosen, for each fit. [c] Karplus coefficients derived using the X-ray ϕ angles.[30] [d] Karplus coefficients derived using the refined ϕ angles derived from X-ray and NMR data.

and HNCA[HA]-E.COSY spectra and, as pointed out previously,[32] they tend to systematically underestimate their true values. Values measured with the three methods are compared in Figure 2. Sixty three non-glycine $^3J_{H^NH^\alpha}$ couplings could be extracted from the *J*-modulated data and 62 non-glycine values from the 3D HNHA spectrum. Due to a rather high incidence of overlap in the C^α dimension of the HNCA[HA]-E.COSY spectrum, only 45 non-glycine couplings could be extracted from this spectrum. The 3D HNHA spectrum also gives the two individual $^3J_{H^NH^\alpha}$ values for each glycine residue, but these values need to be corrected separately for the relatively efficient $H^{\alpha 2}-H^{\alpha 3}$ spin flip−flop events.[21,31] As these values are not easily measured from the CT-HMQC and HNCA[HA]-E.COSY experiments, and as the substituent pattern at C^α is unique, these values are not included in the analysis and a discussion of the ϕ dependence of glycine $^3J_{H^NH^\alpha}$ couplings will be presented elsewhere.

After correcting each of the HNCA[HA]-E.COSY $^3J_{H^NH^\alpha}$ couplings for its finite $T_{1\alpha}$ value (dashed *vs* solid line in Figure 2A), the pairwise rmsd with the CT-HMQC $^3J_{H^NH^\alpha}$ values is 0.29 Hz. After adding a constant 0.4 Hz to the HNHA-derived $T_{1\alpha}$-corrected $^3J_{H^NH^\alpha}$ values,[32] the pairwise rmsd with the CT-HMQC derived values is 0.18 Hz. The pairwise rmsd between the readjusted HNHA and the corrected HNCA[HA]-E.COSY data is 0.27 Hz.

Although the CT-HMQC $^3J_{H^NH^\alpha}$ values clearly are extremely reproducible, the possibility of small systematic errors cannot be excluded. However, as pointed out in the legend to Figure 6, the deviations from the $^3J_{H^NH^\alpha}$ Karplus curve correlate best with those of the complementary heteronuclear *J* couplings when using CT-HMQC data (rather than HNHA-derived *J* couplings), confirming that the CT-HMQC $^3J_{H^NH^\alpha}$ data have the smallest random error. As they are also the most complete set of $^3J_{H^NH^\alpha}$ values, they were used in all further analyses. The $^3J_{H^NH^\alpha}$ values fall in the 2.4−10.3-Hz range. The coefficients *A*, *B*, and *C* of the Karplus equation, $^3J_{H^NH^\alpha} = A\cos^2(\phi - 60°) + B\cos(\phi - 60°) + C$, were calculated by using singular value decomposition (SVD) to calculate the best fit between the Karplus equation and the ($\phi_{X\text{-ray}}$, $^3J_{H^NH^\alpha}$) data set, where $\phi_{X\text{-ray}}$ refers to the ϕ angles derived from the X-ray structure. The resulting coefficients are listed in Table 1. The validity of the assumption that the $H^N-N-C^\alpha-H^\alpha$ dihedral angle equals $\phi - 60°$ will be analyzed in the discussion section. The motionally averaged N- and C-terminal residues were not used in the fits and therefore the data set consisted of 60 total data points. The uncertainty in the coefficients is assessed by refitting the ($\phi_{X\text{-ray}}$,$^3J_{H^NH^\alpha}$) data set 1000 times, each time omitting 10% of the data points, chosen randomly[9,31] (Table 1). Using $\phi_{X\text{-ray}}$ angles,[30] the rmsd between the Karplus curve and the experimental $^3J_{H^NH^\alpha}$ values is 0.53 Hz. This Karplus curve, the measured data points, and the range of Karplus curves within two standard deviations of the best fit obtained from the 1000 fits are shown in Figure 4A. Although most previously proposed parametrizations for this coupling[3,4,7,8,16,31,48,49] are very similar, the present one is closest to the one derived by Pardi et al.[8] using pancreatic trypsin inhibitor (BPTI). Because the values derived by Pardi et al. were not adjusted for the finite lifetime of the H^α spin state, the present parametrization yields *J* values that are slightly larger in the $\phi = -120°$ region. For the rapidly tumbling BPTI protein,[50] neglecting the $T_{1\alpha}$ correction amounts to a very small attenuation, on the order of a few tenths of a hertz.

Measurement of $^3J_{H^\alpha C'}$. The $^3J_{H^\alpha C'}$ values were measured using both an E.COSY and a quantitative *J* correlation experiment. The HCAN[C′]-E.COSY pulse sequence is shown in Figure 2 (supporting information). This experiment detects the H^α spin during data acquisition and is thus performed most easily when the protein is dissolved in D_2O. The corresponding 3D spectrum correlates the intraresidue $^1H^\alpha$, $^{13}C^\alpha$, and ^{15}N resonances in the three orthogonal dimensions. Since care is taken not to perturb the $^{13}C'$ spin state between ^{15}N evolution and ^1H detection, the ^{15}N resonance is split by the $^1J_{NC'}$ coupling (14.8 ± 0.5 Hz),[14,51] and in the H^α dimension the two components are displaced relative to one another by $^3J_{H^\alpha C'}$ (Figure 1B). As the T_1 relaxation time of the passive spin ($^{13}C'$) is relatively long (>∼1 s), the correction needed for passive spin flips is very small (<∼0.1 Hz) and has been ignored in this study. The HCAN[C′]-E.COSY spectrum also shows cross peaks between $^1H^\alpha$ and $^{13}C^\alpha$ of residue *i*, and the ^{15}N of $i + 1$, which result from transfer via the medium sized $^2J_{NC^\alpha}$ coupling (7 ± 2 Hz).[14] In this latter case, the relative displacement of the two doublet components in the ^1H dimension equals $^2J_{H^\alpha C'}$.

In the HCAN experiment and its E.COSY variant, magnetization starts on $^1H^\alpha$ and is transferred via the $^{13}C^\alpha$ nucleus to ^{15}N. The transfer of magnetization from $^{13}C^\alpha$ to ^{15}N is inefficient as it requires a relatively long dephasing delay (27 ms), and during this dephasing the $^{13}C^\alpha$ magnetization decays relatively rapidly due to its fast transverse relaxation rate, $R_{2,C\alpha}$ ($R_{2,C\alpha} \approx (4.5 \times 10^9)\tau_c$). After ^{15}N evolution, magnetization is transferred back to $^{13}C^\alpha$ where it again requires the long refocusing period. A significant loss in magnetization occurs during this experiment and its use is therefore limited to relatively small proteins, with short rotational correlation times, τ_c. A different pulse sequence, also designed to measure the vicinal $^3J_{H^\alpha C'}$ coupling, was recently proposed by Löhr and Rüterjans.[26] In their experiment magnetization is transferred from $^1H^N$ to $^1H^\alpha$, requiring the protein to be dissolved in H_2O. Intrinsically, this latter experiment is expected to be less affected by rapid $^{13}C^\alpha$ transverse relaxation and therefore to yield higher sensitivity when applied to larger proteins. However, it requires detection of $^1H^\alpha$ during data acquisition which in our hands makes it difficult to accurately measure $^3J_{H^\alpha C'}$ splittings for H^α protons that resonate in the immediate vicinity of the intense H_2O resonance.

The HCAN[C′]-E.COSY experiment was repeated twice and the rms pairwise difference for 62 nonterminal $^3J_{H^\alpha C'}$ values in the two measurements was 0.25 Hz, indicating a random error of 0.13 Hz in the averaged values. Figure 4B shows the

(48) Ramachandran, G. N.; Chandrasekaran, R.; Kopple, K. D. *Biopolymers* **1971**, *10*, 2113−2131.
(49) Smith, L. J.; Sutcliffe, M. J.; Redfield, C.; Dobson, C. M. *Biochemistry* **1991**, *30*, 986−996.
(50) Szyperski, T.; Luginbühl, P.; Otting, G.; Güntert, P.; Wüthrich, K. *J. Biomol. NMR* **1993**, *3*, 151−164.
(51) Juranić, N.; Ilich, P. K.; Macura, S. *J. Am. Chem. Soc.* **1995**, *117*, 405−410.

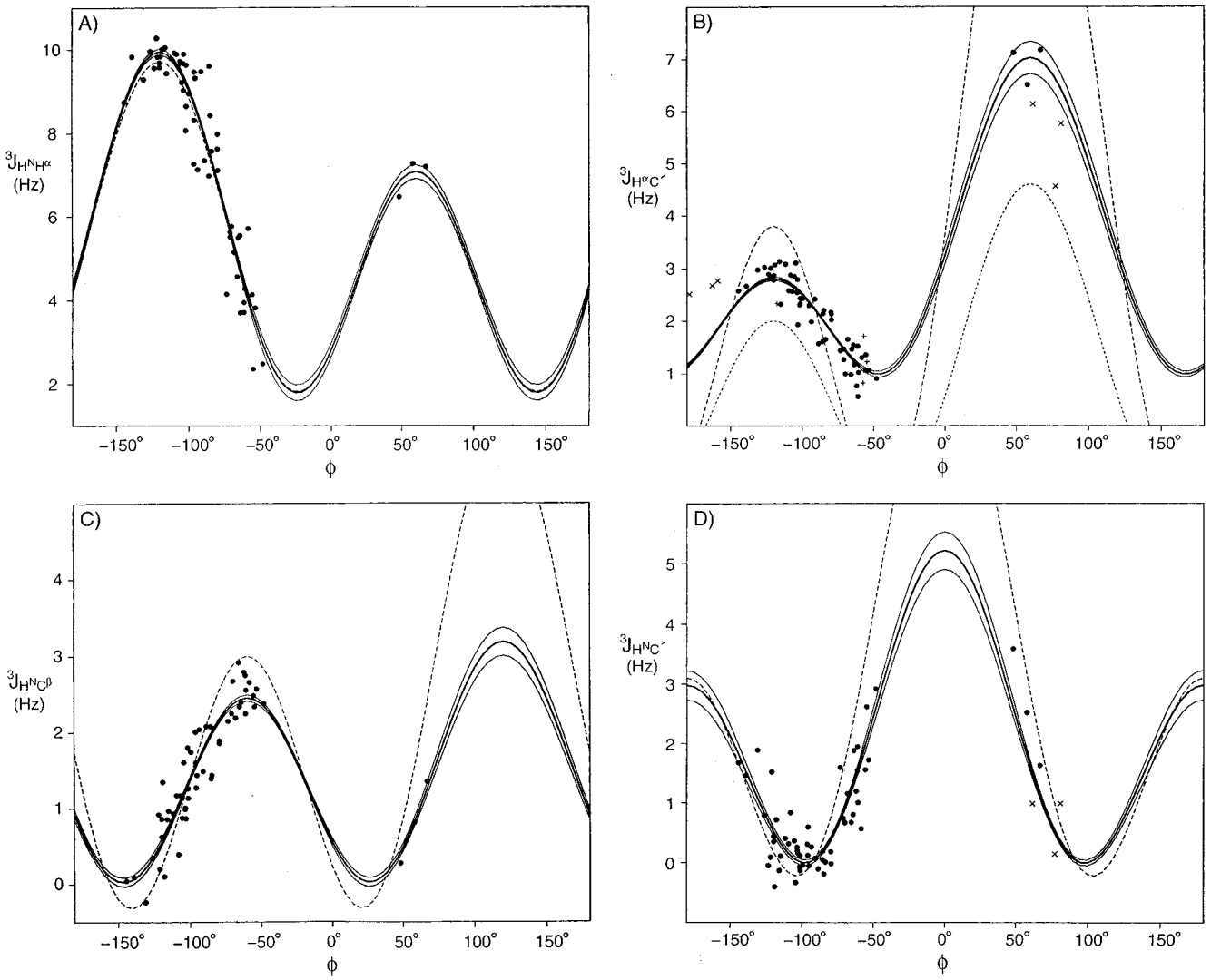

Figure 4. Reparametrized Karplus curves for (A) $^3J_{H^NH^\alpha}$, (B) $^3J_{H^\alpha C'}$, (C) $^3J_{H^NC^\beta}$, and (D) $^3J_{H^NC'}$, calculated using singular value decomposition on the measured couplings and corresponding ϕ angles derived from the X-ray structure. The best fit to the data is shown as a thick solid line, and the thin solid lines are plotted at ±2 standard deviations, calculated from repeating the fit 1000 times with 10% of the points, chosen randomly, omitted for each fit. Dashed lines represent previous parametrizations from (A) Pardi et al.,[8] (B) Bystrov,[4] based on experimental data (longer dashes) and on FPT-INDO theoretical calculations (shorter dashes), and (C and D) FPT-INDO theoretical calculations by Bystrov.[4] In all four plots, the ● symbols mark *J* values for those residues which have at least three measured *J* couplings and were the only ones later subjected to ϕ angle refinement. In part B, the + symbols mark residues for which only the $^3J_{H^\alpha C'}$ coupling could be measured, including three Pro residues. The × symbols mark the *J* values measured for Gly residues. Glycine couplings were included for reparametrizing the $^3J_{H^NC'}$ curve only and were never subjected to ϕ angle refinement.

correlation between these averaged $^3J_{H^\alpha C'}$ values and the X-ray dihedral angle ϕ. The coefficients *A*, *B*, and *C* of the Karplus equation, $^3J_{H^\alpha C'} = A\cos^2(\phi - 60°) + B\cos(\phi - 60°) + C$, were calculated from a best fit of the ($\phi_{X\text{-ray}}$,$^3J_{H^\alpha C'}$) data set using SVD, and these coefficients are listed in Table 1. The rms difference between measured *J* splittings and values predicted on the basis of this curve (Figure 4B) is 0.25 Hz.

A second set of $^3J_{H^\alpha C'}$ values was obtained from recording a 3D HN(CO)HB quantitative *J* correlation spectrum.[22,35] This experiment was originally developed for measuring $^3J_{H^\beta C'}$ couplings, and it yields a 3D spectrum in which correlations are observed between the H^N (F_3 dimension) and ^{15}N (F_1 dimension) of residue *i* and H^N, H^α, and H^β of $i - 1$ (F_2 dimension), in addition to correlations with H^N (F_2/F_3 diagonal) and H^α of residue *i*. The intensities of these correlations are related in a simple manner to the size of the *J* coupling between these protons and the carbonyl carbon, $^{13}C'$, of residue $i - 1$.[22,35] Except for $^1H-^1H$ spin flips during the $^{13}C'$ de- and rephasing periods, the effect of relaxation during the HN(CO)HB pulse scheme is accounted for by also recording a 2D $^1H^N-^{15}N$ reference spectrum, using a 2D analog of the 3D HN(CO)HB pulse sequence, in which magnetization is subjected to the same relaxation processes that apply to the 3D case.[22] In fact, it is the ratio of the intensity of a correlation in the 3D experiment (I_{3D}) to the corresponding $^1H^N-^{15}N$ correlation intensity in the 2D reference spectrum (I_{2D}) that is used for determining the value of the $^1H-^{13}C'$ *J* coupling from the relation[22]

$$I_{3D}/I_{2D} = A\tan^2(\pi J_{HC'}\Delta) \qquad (2)$$

where Δ is the duration of the delays in the pulse scheme during which $^{13}C'$ magnetization dephases and rephases with respect to its long-range coupled protons. Besides the digital filtering, the number of scans used in the 2D and 3D experiments, and the number of increments used in the indirect proton dimension of the 3D experiment, the constant *A* also depends on the lifetime of the $^1H^\alpha$ spin.[21,31,52] This latter contribution is not

(52) Vuister, G. W.; Bax, A. *J. Magn. Reson. Ser. B* **1993**, *102*, 228−231.

negligible because, as discussed above, $T_{1\alpha}$ is relatively short due to $^1H-^1H$ spin flips. The constant A can be easily calibrated by using the intraresidue $^2J_{H^\alpha C'}$ couplings as a reference: These $^2J_{H^\alpha C'}$ couplings are measured from the same 3D HN(CO)HB spectrum and then compared to those from a 2D CT-HSQC E.COSY-type spectrum in which the spin state of the $^{13}C'$ nuclei is not perturbed.[18] The constant A has the value that minimizes the rms difference between the two sets of measurements. The good agreement between the two sets of $^2J_{H^\alpha C'}$ couplings is shown in Figure 7 in the supporting information, and the pairwise rms differences between the $^2J_{H^\alpha C'}$ values derived from the HSQC-E.COSY spectrum and HN(CO)HB spectra recorded at 600 and 500 MHz ^1H frequencies are 0.32 and 0.24 Hz, respectively.

For 48 residues, the HN(CO)HB spectrum yielded J connectivity between $^{13}C'$ of residue $i-1$ and $^1H^\alpha$ of residue i that fell above the detection threshold. The pairwise rmsd between the 500 and 600 MHz $^3J_{H^\alpha C'}$ values is 0.19 Hz, indicating a random error of 0.1 Hz in the averaged value. The pairwise rms difference between the values measured with the HCAN[C′]-E.COSY experiment and the HN(CO)HB experiment is 0.27 Hz. This relatively large pairwise rmsd between E.COSY and HN(CO)HB derived ^3J values may be caused in part by the implicit assumption of a uniform value for $T_{1\alpha}$ when empirically deriving A for eq 2. As several of the $^3J_{H^\alpha C'}$ values fall below the detection threshold in the HN(CO)HB experiment, and as a considerably larger set of $^3J_{H^\alpha C'}$ values could be derived from HCAN[C′]-E.COSY which also lack significant distortion caused by the finite values of $T_{1C'}$, only the E.COSY data were used in deriving the Karplus parameters (Table 1). The HN(CO)HB data served as a useful check for the absence of large errors from either systematic or random sources.

$^3J_{H^\alpha C'}$ couplings to glycine H^α protons are marked by $\times$ in Figure 4B and were not used in the Karplus curve parametrization. The poor agreement between measured and predicted $^3J_{H^\alpha C'}$, as mentioned above, could be caused by the different C^α substituent pattern of glycines and/or by unusually large differences with the X-ray ϕ angles of these residues.

Measurement of $^3J_{H^N C^\beta}$. Since many $^3J_{H^N C^\beta}$ couplings are quite small, they are most easily measured using an E.COSY-type experiment. In our present study we have used a variant of the HNCA-E.COSY pulse sequence,[33] in which $^{13}C^\beta$ is the passive spin. Therefore, this pulse scheme requires a selective 90° pulse, applied to the C^α region of the ^{13}C spectrum, between $^{13}C^\alpha$ evolution and $^1H^N$ detection. As serine C^β carbons also resonate in this spectral region, their $^3J_{H^N C^\beta}$ values are unreliable. This HNCA[CB]-E.COSY pulse sequence is shown in Figure 4 in the supporting information and the pulse sequence code is also available as supporting information. Alternative methods for measuring $^3J_{H^N C^\beta}$ have recently been proposed by Seip et al.[24] and by Löhr and Rüterjans.[26]

Figure 1C shows experimental data obtained with the HNCA[CB]-E.COSY experiment for residues $Leu^{43}-Ala^{46}$. The 60 $^3J_{H^N C^\beta}$ couplings, extracted from the spectrum, fall in the -0.2 to 2.9 Hz range (Figure 4C). As the pairwise rms difference between values measured from two separate 3D experiments is 0.29 Hz, the rms error in the average value of $^3J_{H^N C^\beta}$ is *ca.* 0.15 Hz. The coefficients A, B, and C of the Karplus equation, $^3J_{H^N C^\beta} = A\cos^2(\phi + 60°) + B\cos(\phi + 60°) + C$, were calculated from a best fit of the ($\phi_{X\text{-ray}}$,$^3J_{H^N C^\beta}$) data set using SVD, and these coefficients are listed in Table 1. As three residues near the N- and C-termini are subject to motional averaging, 57 couplings were used in the reparametrization. The rms difference between measured J splittings and values predicted on the basis of this curve is 0.24 Hz. The relatively small value of the *trans* coupling ($\phi = 120°$) suggested by our reparametrized curve is primarily caused by three residues with positive ϕ angles (Ala^{46}, Asn^{60}, and Glu^{64}) which, as will be shown later on the basis of the other ^3J couplings measured for these residues, each have ϕ angles that are somewhat smaller in solution than in the crystalline state. As will be discussed later, use of the refined ϕ angles results in a Karplus curve with larger *trans* couplings, closer to the original parametrization[4] (Table 1).

Measurement of $^3J_{H^N C'}$. Values for $^3J_{H^N C'}$ in ubiquitin have been measured previously using an HNCA[C′]- E.COSY-type triple resonance experiment.[9] Measured values fall in the -0.4 to 3.6 Hz range and the rms error in the measured data was 0.1 Hz. Values for $^3J_{H^N C'}$ can also be obtained from the 3D HN(CO)HB quantitative J correlation spectrum, which was used above for measurement of $^3J_{H^\alpha C'}$. However, under the experimental conditions chosen, only $^3J_{H^N C'}$ couplings that are larger than about 1 Hz give rise to observable cross peaks. Therefore, only 17 $^3J_{H^N C'}$ couplings could be measured quantitatively from the 3D HN(CO)HB spectrum. The pairwise rms difference between these values and the corresponding couplings measured from the 3D HNCA[C′]-E.COSY spectrum is 0.30 Hz. Due to overlap in the E.COSY for Glu^{64}, $^3J_{H^N C'}$ for this residue was derived from the two HN(CO)HB spectra. Including this additional data point does not change the Karplus parametrization (Table 1) beyond the uncertainty reported earlier.[9] The rms difference between measured J splittings and values predicted on the basis of this curve (Figure 4D) is 0.36 Hz.

Discussion

The rms agreement between the measured J couplings and values predicted by the corresponding Karplus curves for all four types of couplings is considerably worse than the random uncertainty of these J values. The question then arises whether this disagreement is caused by uncertainties in the 1.8-Å X-ray structure,[30] or whether it reflects the influence of other variables on the J coupling, such as the nature of the amino acid side chain, the strength of the hydrogen bond to the backbone amide, or the influence of backbone motions[53,54] (*vide infra*). A further possibility which will be analyzed below is that our assumption that the amide proton is located in the $C'_{i-1}-N_i-C^\alpha_i$ plane is invalid.[55,56]

Bartik et al.[29] previously noted in their study of lysozyme that the rms difference between measured $^3J_{H^N H^\alpha}$ values and those predicted by the Karplus curve of Pardi et al.[8] decreased significantly with increasing resolution of the lysozyme X-ray structure, strongly suggesting that uncertainties in the ϕ angles of the X-ray structures solved at resolutions of 2.2 and 2.5 Å contribute significantly to the difference between measured and predicted J values. For the highest resolution X-ray structure (1.5 Å), Bartik et al.[29] reported a rms difference of 0.8 Hz between measured and predicted values, somewhat larger than the 0.53-Hz difference reported above for our ubiquitin study. Similarly, the rms differences between measured and predicted J couplings for BPTI were 0.85 and 0.65 Hz, using X-ray structures solved at 1.4- and 0.94-Å resolution.[8]

(53) Hoch, J. C.; Dobson, C. M.; Karplus, M. *Biochemistry* **1985**, *24*, 3831−3841.
(54) Brüschweiler, R.; Case, D. A. *J. Am. Chem. Soc.* **1994**, *116*, 11199−11200.
(55) Head-Gordon, T.; Head-Gordon, M.; Frisch, M. J.; Brooks, C. L., III; Pople, J. A. *J. Am. Chem. Soc.* **1991**, *113*, 5989−5997.
(56) Edison, A. S.; Weinhold, F.; Westler, W. M.; Markley, J. L. *J. Biomol. NMR* **1994**, *4*, 543−551.
(57) Taylor, J. R. *An Introduction to Error Analysis the Study of Uncertainties in Physical Measurements*; University Science Books: Mill Valley, CA, 1982.

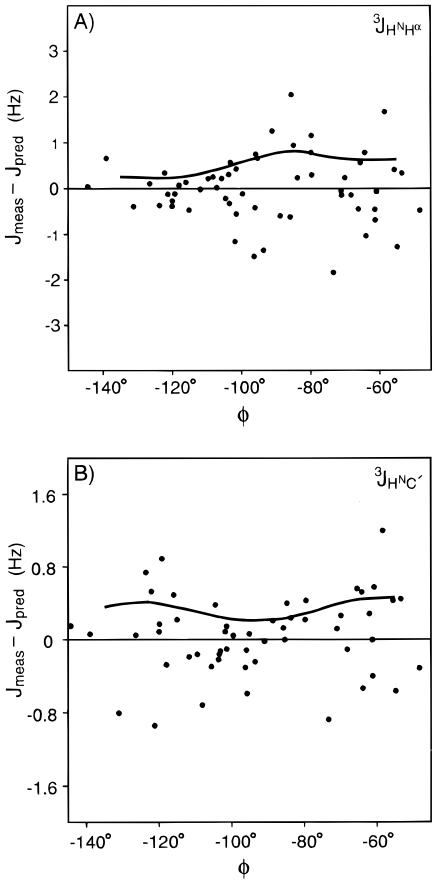

Figure 5. Plots of the deviation between measured J values, J_{meas}, and those predicted by the Karplus curve, J_{pred}, for (A) $^3J_{H^NH^\alpha}$ and (B) $^3J_{H^NC'}$ using X-ray ϕ angles. The average absolute deviation (solid line), $\Delta_{\delta J}(\phi)$, is calculated by convoluting the absolute value of $\delta_J{}^k(\phi) = J_{meas}{}^k - J_{pred}{}^k$ for each residue, k, with the center lobe of a cosine function, prior to addition and normalization: $\Delta_{\delta J}(\phi) = \sum_k|\delta_J(\phi)|\ \mathrm{cosb}[(\phi - \phi_k)w]/\sum_k \mathrm{cosb}[(\phi - \phi_k)w]$, where cosb denotes a cosine bell function with $\mathrm{cosb}(\theta) = \cos(\theta)$ for $|\theta| < 90°$, and $\mathrm{cosb}(\theta) = 0$ for $|\theta| > 90°$. The summation extends over all residues, k, and the width, w, was arbitrarily chosen to equal 4.5, yielding a ±20° cosine bell.

Small changes in the ϕ angle have very little effect on the predicted $^3J_{H^NH^\alpha}$ value where the derivative of the Karplus equation is small (*i.e.*, for $\phi \approx -120° + n \times 90°$), and the effects are large where the derivative of the Karplus curve increases. Figure 5A shows, as a function of ϕ, the difference between measured $^3J_{H^NH^\alpha}$ values and those predicted by the Karplus curve, for the region where the curve is clearly overdetermined. The heavy line in this figure represents the local rms difference between the measured J values and the Karplus curve and it increases with the steepness of the Karplus curve. A similar discrepancy is observed between predicted and measured $^3J_{H^NC'}$ couplings (Figure 5B) and, to a lesser extent, also for the $^3J_{H^\alpha C'}$ and $^3J_{H^NC^\beta}$ couplings (Figure 8, supporting information). Most importantly, however, for ϕ angles where the derivative of the applicable Karplus equation is small, the average discrepancy between measured and predicted values approaches our estimate for the error in the measurement of J and increases where the derivative is larger. This strongly suggests that small differences between the X-ray ϕ angles and those present in the solution state are a main source for the difference between measured and predicted J values. These small differences in ϕ angles may reflect the uncertainties in the X-ray structure but can also contain a real component resulting from crystal packing forces.

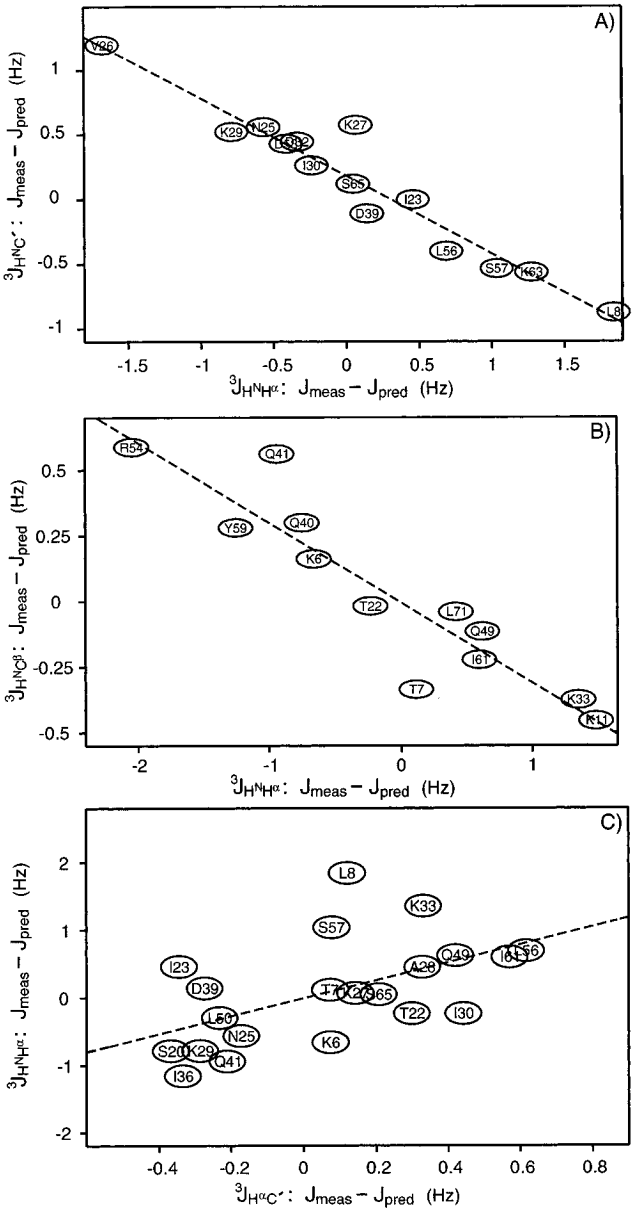

Figure 6. Correlation plot of $\delta_J = J_{meas} - J_{pred}$, derived using $\phi_{X\text{-ray}}$ angles, between (A) $^3J_{H^NH^\alpha}$ and $^3J_{H^NC'}$ in the range $-75° \le \phi \le -50°$, (B) $^3J_{H^NH^\alpha}$ and $^3J_{H^NC^\beta}$ in the range $-100° \le \phi \le -80°$, and (C) $^3J_{H^NH^\alpha}$ and $^3J_{H^\alpha C'}$ in the range $-100° \le \phi \le -60°$. The statistical significance of these correlations[57] is described by the correlation coefficients, r, defined by $r = \sum_i [(x_i - x_{ave})(y_i - y_{ave})]/[\sum(x_i - x_{ave})^2\sum(y_i - y_{ave})^2]^{1/2}$. These r values are (A) 0.96, (B) 0.92, and (C) 0.54, and the conditional probabilities, P, that these correlations result from random uncertainties[57] are 4×10^{-8}, 2×10^{-5}, and 1×10^{-2}, respectively. When using $^3J_{H^NH^\alpha}$ values and a corresponding Karplus curve derived from the HNHA experiment, these r values drop to 0.95, 0.90, and 0.50, respectively (data not shown).

If the difference between measured and predicted J values, $\delta_J(\phi) = J_{meas}(\phi) - J_{pred}(\phi)$, is dominated by the uncertainty in the ϕ angle, $\delta_J(\phi)$ values for $^3J_{H^NC'}$ and $^3J_{H^NH^\alpha}$ are expected to be strongly correlated in regions where both Karplus curves have a steep ϕ dependence. Indeed, as shown in Figure 6, such a strong correlation is clearly observed, not only between $^3J_{H^NC'}$ and $^3J_{H^NH^\alpha}$, but also between $^3J_{H^NH^\alpha}$ and $^3J_{H^NC^\beta}$, and between $^3J_{H^NH^\alpha}$ and $^3J_{H^\alpha C'}$. This indicates that the deviations between measured and predicted J values are in fact dominated by small differences between the ϕ angles derived from the X-ray structure and those prevailing in solution. An alternative explanation for the correlations shown in Figures 6A and 6B

(but not Figure 6C) could be that H^N is located above or below the plane defined by C'_{i-1}, N_i, and C^α, i.e., that the $H^N-N-C^\alpha-H^\alpha$ torsion angle deviates from $\phi - 60°$. However, considering that there appears to be little or no correlation between the predicted deviation from $\phi - 60°$ and the experimentally measured deviation (*vide infra*), this effect presumably is very small.

Accuracy of X-ray ϕ Angles. <sen>The random deviation between measured and predicted J values, $\delta_J(\phi)$, increases in regions where the Karplus equation has its steepest ϕ angle dependence, most notably for $^3J_{H^NH^\alpha}$ and $^3J_{H^NC'}$ (Figure 5), and to a lesser extent also for $^3J_{H^\alpha C'}$ and $^3J_{H^NC^\beta}$ (Figure 8, supporting information). Contributions to $\delta_J(\phi)$ may be split in two groups: a contribution $\delta_\phi(\phi)$ stems from the uncertainty in the X-ray ϕ angles and/or from small differences between the ϕ angle in the crystalline and solution state of the protein; and a contribution, $\delta_{o.f.}(\phi)$, caused by other factors such as measurement error, backbone dynamics, or hydrogen bonding. If $\delta_\phi(\phi)$ and $\delta_{o.f.}(\phi)$ are assumed to be independent of one another, the following relation applies:

$$\delta_J(\phi) = [\delta_{o.f.}(\phi)^2 + \delta_\phi(\phi)^2]^{1/2} \quad (3)$$

The value of $\delta_\phi(\phi)$ for $^3J_{H^NH^\alpha}$ is zero near $\phi = -120°$, and $\delta_{o.f.}(-120°)$ is estimated from Figure 5A to be 0.24 Hz. For $\phi = -73°$, $\delta_J(\phi)$ is 0.67 Hz and eq 3 then indicates that $\delta_\phi(-73°)$ is 0.63 Hz. Since the derivative of the $^3J_{H^NH^\alpha}$ Karplus equation in this region is -0.13 Hz per degree, there is a random uncertainty of $\pm 4.8°$ in the X-ray ϕ angle. Similarly, for $^3J_{H^NC'}$ the value of $\delta_{o.f.}(\phi)$ is estimated from Figure 5B to equal 0.21 Hz (at $\phi = -98°$), $\delta_\phi(\phi)$ equals 0.40 Hz at $\phi = -60°$, and the derivative of the Karplus curve is 0.078 Hz per degree at $\phi = -60°$. This indicates a rms difference of 5.1° between the X-ray and solution structure ϕ angles. The presence of these small differences is not surprising, considering that the rms deviation between backbone ϕ angles of a given protein, solved independently in different laboratories, typically is on this order of magnitude. For example, excluding residues with high-temperature factors, the rms difference in the ϕ angles is 4.7° between two X-ray structures of BPTI, solved at resolutions of 1.0 and 1.1 Å[58,59] in the same crystal form.

Our coupling constant data (Figure 6) suggest that the NMR J couplings may be used to refine the X-ray ϕ angle so as to minimize the difference between the measured $^3J_{H^NC'}$, $^3J_{H^NC^\beta}$, $^3J_{H^\alpha C'}$, and $^3J_{H^NH^\alpha}$ values and their respective Karplus curves. For each residue the function

$$\chi^2(\phi) = \sum[^3J_{meas} - {}^3J_{pred}(\phi) \pm \delta_{o.f.}]^2/E^2 \quad (4)$$

is minimized, where the summation extends over all J couplings measured for a given residue, E is the rms difference between measured and predicted values (0.53 Hz for $^3J_{H^NH^\alpha}$, 0.24 Hz for $^3J_{H^NC^\beta}$, 0.36 Hz for $^3J_{H^NC'}$, and 0.25 Hz for $^3J_{H^\alpha C'}$), and $\delta_{o.f.}$ is 0.24 Hz for $^3J_{H^NH^\alpha}$, 0.18 Hz for $^3J_{H^NC^\beta}$, 0.21 Hz for $^3J_{H^NC'}$, and 0.22 Hz for $^3J_{H^\alpha C'}$. The "$+\delta_{o.f.}$" term in square brackets in eq 4 is used if $(^3J_{meas} - {}^3J_{pred}(\phi)) < -\delta_{o.f.}$; a "$-\delta_{o.f.}$" term is used if $^3J_{meas} - {}^3J_{pred}(\phi) > \delta_{o.f.}$. The term in square brackets is set to zero if $|^3J_{meas} - {}^3J_{pred}(\phi)| \le \delta_{o.f.}$. This has the same effect as the so-called square-well potential function used in the XPLOR[60,61] protein structure calculation program, where distances outside allowed, experimentally derived ranges provide a driving force for altering the structure. Therefore, use of eq 4 does not modify the X-ray ϕ angles by more than is necessary to bring the J couplings within the experimental error of the Karplus curve. The $\phi_{X\text{-ray}}$ and refined ϕ angles (ϕ_{ref}) are listed in Table 2 in the supporting information. The rms difference between the two sets of ϕ angles is 5.7°. After refining the ϕ angles in the manner described above, the rms differences between measured and predicted J couplings drop from 0.53 to 0.22 Hz for $^3J_{H^NH^\alpha}$, from 0.36 to 0.21 Hz for $^3J_{H^NC'}$, from 0.24 to 0.14 Hz for $^3J_{H^NC^\beta}$, and from 0.25 to 0.21 Hz for $^3J_{H^\alpha C'}$. The Karplus curves resulting from fitting the four (ϕ_{ref},^3J) data sets as described above are shown in Figure 7. The ϕ angles can also be calculated from the NMR data alone (Table 2, supporting information) and are very close to the ϕ angles obtained when combining the X-ray and NMR information (rmsd = 0.8°).

The differences between the crystal and solution ϕ angles appear to be random and, with the exception of $^3J_{H^NC^\beta}$, reparametrization of the Karplus curves using ϕ_{ref} (instead of $\phi_{X\text{-ray}}$) does not result in large changes of the Karplus parameters (Table 1). For $^3J_{H^NC^\beta}$, the region of the Karplus curve for positive ϕ angles is primarily determined by only three residues, and use of the refined ϕ angles results in a significant change in this region of the curve (Figure 7C), removing the unusual feature of heteronuclear *trans* couplings that are comparable in magnitude to the *cis* values (Figure 4C).

Relation between ϕ and Torsion Angles Involving H^N. When the Karplus curves for $^3J_{H^NH^\alpha}$, $^3J_{H^NC'}$, and$^3J_{H^NC^\beta}$ were reparametrized, an implicit assumption was made that H^N is located in the plane defined by C'_{i-1}, N_i, and C^α. However, *ab initio* calculations carried out on a dipeptide analog in vacuum suggest that, depending on the values of ϕ and ψ, large deviations from this idealized geometry will occur.[55,56] According to these *ab initio* calculations, in ubiquitin the differences, Δ_{ai}, between the calculated $H^N-N-C^\alpha-C'$ dihedral angles and $\phi - 180°$ are as large as 25° and these Δ_{ai} values are presented in Table 4 in the supporting information. However, using the dihedral angles obtained from these *ab initio* calculations instead of the idealized $\phi \pm 60°$ or $\phi - 180°$ dihedral angles to parametrize the Karplus curves results in a poorer fit, with a significant increase in the rms difference between measured and predicted $^3J_{H^NH^\alpha}$ values. However, as shown in Figure 8, when the correction Δ_{ai} is scaled by a factor f, the rms fit shows a very small improvement for $^3J_{H^NC'}$ for an f value of 0.1.

Neglecting the possible distortion from tetrahedral geometry at the C^α carbon, a second way for investigating the effect of the nonplanarity of the peptide bond is to compare, in the manner of Figure 6C, the correlation between deviations between $^3J_{H^\alpha C'}$ values and their Karplus curve with those between $^3J_{H^NH^\alpha}$ and Karplus curves derived as a function of f. As shown in Figure 9 in the supporting information, the correlation coefficient, r, increases from 0.54 for $f = 0$ to a maximum of 0.57 for $f = 0.15$.

The results presented in Figure 8 and in Figure 9 in the supporting information suggest that taking into account the difference between $\phi - 60°$ and the $H^N-N-C^\alpha-H^\alpha$ dihedral angle does not result in significantly better fits between the J couplings and the ϕ angles derived from the ubiquitin X-ray structure. As shown in Figure 10 in the supporting information, there appears to be no significant correlation between the Δ_{ai} values and the corrections to the X-ray ϕ angle calculated from the NMR data (Table 4, supporting information).

(58) Wlodawer, A.; Walter, J.; Huber, R.; Sjölin, L. *J. Mol. Biol.* **1984**, *180*, 301−329.
(59) Parkin, S.; Rupp, B.; Hope, H. *Acta Crystallogr. D* In press.
(60) Clore, G. M.; Nilges, M.; Sukumaran, D. K.; Brünger, A. T.; Karplus, M.; Gronenborn, A. M. *EMBO J.* **1986**, *5*, 2729−2735.
(61) Brünger, A. T. *X-PLOR Version 3.1: A System for X-ray Crystallography and NMR*; Yale University Press: New Haven, CT, 1992.

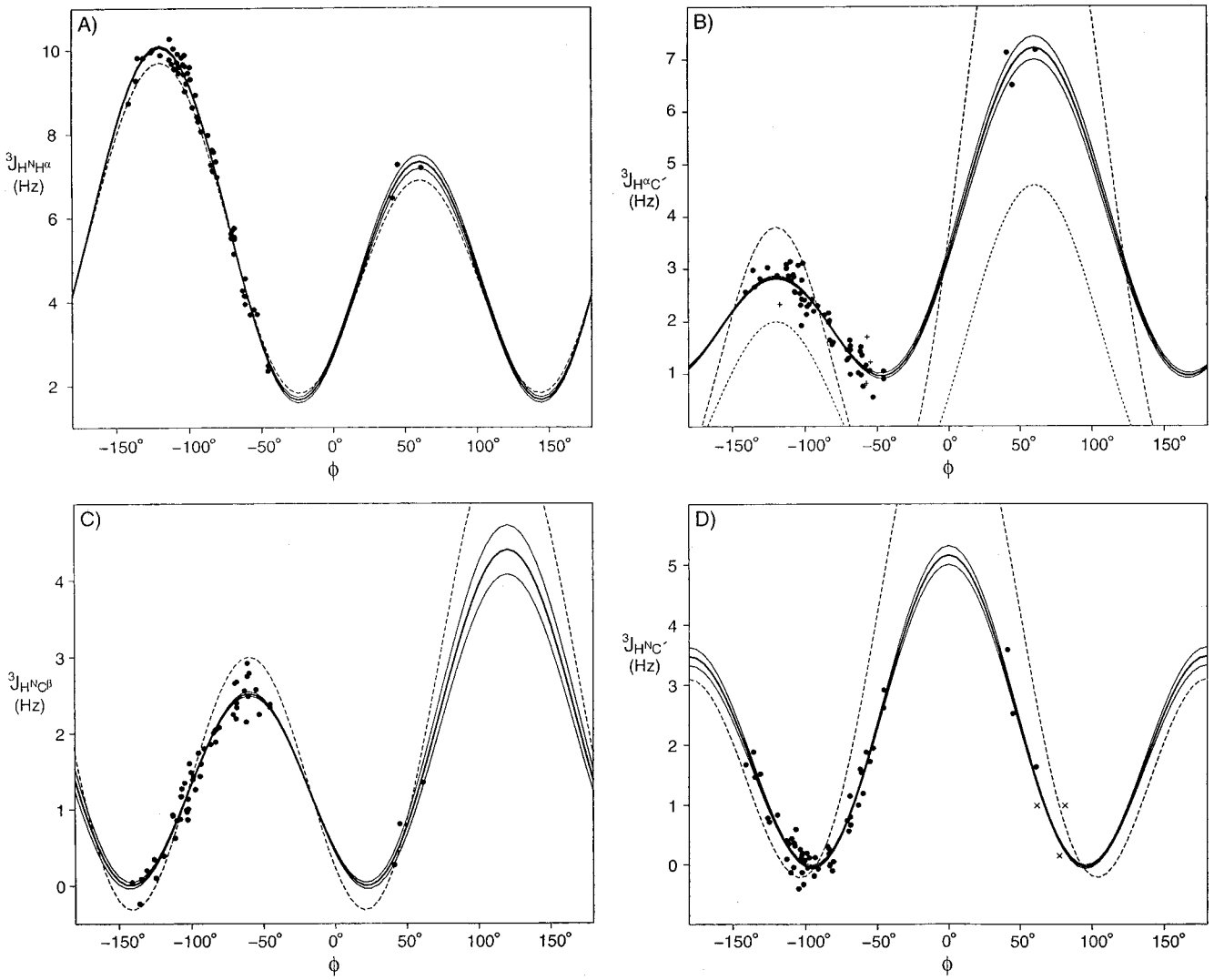

Figure 7. Reparametrized Karplus curves for (A) $^3J_{H^NH^\alpha}$, (B) $^3J_{H^\alpha C'}$, (C) $^3J_{H^NC^\beta}$, and (D) $^3J_{H^NC'}$ after backbone ϕ angle refinement, as described in the text. The ● symbols mark J values for residues which have at least three measured J couplings and were subjected to ϕ angle refinement. The + symbols mark residues for which only the $^3J_{H^\alpha C'}$ coupling could be measured, including three Pro residues, and were not subject to ϕ angle refinement. The × symbols mark J values measured for Gly residues (no ϕ angle refinement) and were only used in parametrization of the $^3J_{H^NC'}$ Karplus curve. The best fit to the data is shown as a thick solid line and the thin solid lines are plotted at ±2 standard deviations calculated from 1000 fits, each with 10% of the J values, randomly chosen, omitted. Dashed lines represent previous parametrizations (see legend to Figure 4).

Assuming that the tetrahedral geometry at the C^α carbon is not influenced by ϕ and ψ, the $C'_{i-1}-N_i-C^\alpha{}_i-H^\alpha{}_i$ dihedral angle is not affected by the planarity of the peptide bond. The correlation between $J_{meas} - J_{pred}$ for $^3J_{H^\alpha C'}$ and $^3J_{H^NH^\alpha}$ (Figure 6C) therefore cannot result from a difference between $\phi - 60°$ and the $H^N-N-C^\alpha-H^\alpha$ dihedral angle. The fact that the correlation coefficient is lower compared to the correlations observed in Figures 6A and 6B suggests that the difference between $\phi - 60°$ and the H^N-N-C^α-H^α dihedral angle may not be negligible, but it also results from the relatively large uncertainty in the measured $^3J_{H^\alpha C'}$ values.

Effect of Intramolecular Motions. As discussed by Hoch et al.,[53] the effect of thermal motions on the value of backbone J couplings in proteins is anticipated to be small. This topic has recently been revisited by Brüschweiler and Case,[54] who showed that in the case where the backbone angle ϕ averages over a population with a Gaussian distribution of amplitude σ ($\sigma \ll \pi$), a Karplus relation, derived hypothetically for a rigid molecule, is modified into

$$J(\phi) = A\exp(-2\sigma^2)\cos^2\phi + B\exp(-\sigma^2/2)\cos\phi + (1 - \exp(-2\sigma^2))A/2 + C \quad (5)$$

The Karplus curve parametrizations in Table 1 are based on a protein in solution at 30 °C, and already include the effects of thermal motion. Assuming arbitrarily that the "true" amplitude of σ is 12°, the parametrization in the absence of motion can be calculated by inverting the Karplus parameter correction factors of eq 5,[54] yielding a curve for $\sigma = 0°$ (Figure 9). In addition to the $\sigma = 0°$ curve, Figure 9 also shows $^3J_{H^NH^\alpha}$ Karplus curve σ values of 12° and 24°. The three curves differ most from one another at $\phi \approx -120°$. As noted above, in this region the rms deviations between the Karplus curve and the measured $^3J_{H^NH^\alpha}$ values are, to first order, independent of small differences between the X-ray and solution structure ϕ angles. Therefore, the residual rms deviation between measured $^3J_{H^NH^\alpha}$ values and the Karplus curve in the $\phi \approx -120°$ region reflects the sum of the errors introduced by variation in the backbone dynamics, the random error in the measurement, and the sensitivity of the $^3J_{H^NH^\alpha}$ value to factors other than ϕ. This puts a stringent limit on the maximum variation of the amplitude of the backbone dynamics: If the true amplitude, σ_{true}, of a given residue in the $\phi \approx -120°$ region were only 6° instead of 12°, the predicted $^3J_{H^NH^\alpha}$ value would increase by 0.26 Hz and if σ were 18°, the predicted $^3J_{H^NH^\alpha}$ value would decrease by 0.40 Hz (*cf.* eq 5).

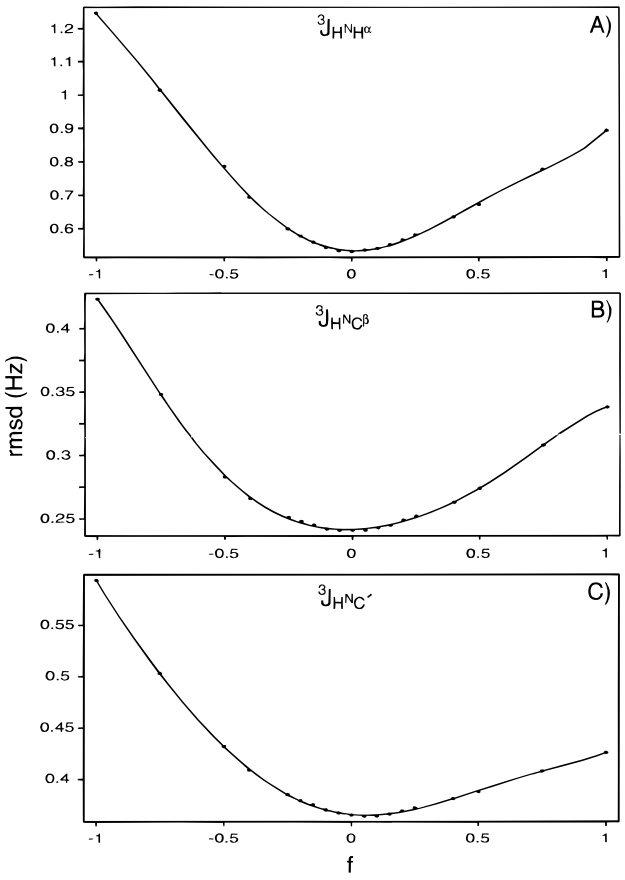

Figure 8. Root-mean-square deviations between measured (A) $^3J_{H^NH^\alpha}$, (B) $^3J_{H^NC^\beta}$, and (C) $^3J_{H^NC'}$ values and best-fit Karplus curves calculated using dihedral angles (A) $\phi - 60° - f\Delta_{ai}$, (B) $\phi + 60° - f\Delta_{ai}$, and (C) $\phi - f\Delta_{ai}$, where ϕ is derived from the X-ray structure, and Δ_{ai} is the (ϕ,ψ)-dependent correction, obtained from the results of *ab initio* calculations, presented in Figure 9 of Head-Gordon et al.[55]

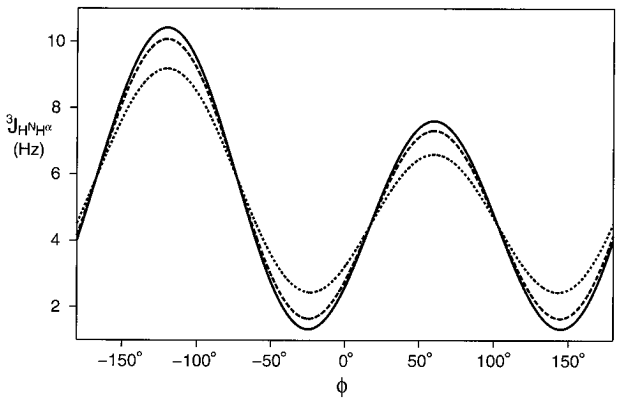

Figure 9. Effect of different ϕ angle fluctuation amplitudes, σ, on the $^3J_{H^NH^\alpha}$ Karplus curve (*cf.* eq 5). For all three curves shown, it is assumed that the original *A*, *B*, and *C* parameters were derived for residues with a σ value of 12°. Therefore, the σ =12° curve (long dashes) is identical to that shown in Figure 7A, and the σ = 0° (solid) and 24° (short dashes) curves are calculated using eq 5.

These differences are comparable to the largest difference between a measured value and the Karplus curve in the $\phi \approx -120°$ region (0.38 Hz using $\phi_{X\text{-ray}}$, and 0.20 using ϕ_{ref}). Thus, in human ubiquitin the amplitude of the ϕ angle fluctuations for residues with $\phi \approx -120°$ must be relatively uniform. As will be discussed elsewhere (A. C. Wang and A. Bax, unpublished results), for most residues in human ubiquitin the temperature dependence of the *J* coupling is extremely small ($\leq$0.005 Hz/°C) and it seems unlikely that the difference in Karplus parametrizations currently in the literature for $^3J_{H^NH^\alpha}$ can be attributed to the different temperatures at which the NMR experiments were conducted.[54]

A 3-ns molecular dynamics study of partially hydrated ubiquitin suggested that the positive ϕ angles observed for Ala[46] and Glu[64] in the X-ray structure of ubiquitin were artifacts of intermolecular contacts in the crystal lattice.[62] In the crystal structure these residues occupy the second position in type III′ and type II reverse turns, respectively. The *J* couplings measured for Ala[46] and Glu[64] are fully compatible with the X-ray structure and rule out the possibility that a second conformer, with a negative ϕ angle, is extensively populated for each of these turns.

Conclusions

The original parametrizations of the Karplus equations for $^3J_{H^NC'}$, $^3J_{H^NC^\beta}$, and $^3J_{H^\alpha C'}$ fall well outside the range of the new parametrizations derived for human ubiquitin. The new parametrizations are the first ones based on extensive experimental data and therefore are expected to be considerably more accurate. The new parametrization for $^3J_{H^NH^\alpha}$ agrees reasonably well with previously proposed curves.[3,4,8,16,31,48,49] All of these curves are rather similar in the region of negative ϕ angles but show increased scatter in the region of positive ϕ angles, where fewer calibration points are available.

The agreement between measured *J* couplings and ϕ angles derived from the X-ray structure decreases when corrections to the pertinent dihedral angles are made to account for the out-of-plane position of the peptide amide proton, predicted by *ab initio* calculations carried out for a dipeptide analog in vacuum, i.e., in the absence of hydrogen bonding. In the absence of such corrections the ϕ angles derived from the X-ray structure already agree with the NMR data to within the combined uncertainties of the X-ray coordinates and the NMR *J* couplings. This indicates that $\phi - 60°$ is a very good approximation for the $H^N-N-C^\alpha-H^\alpha$ dihedral angle.

Our study of $^3J_{H^NC'}$, $^3J_{H^NC^\beta}$, $^3J_{H^\alpha C'}$, and $^3J_{H^NH^\alpha}$, which are all related to the dihedral backbone angle ϕ, suggests that in proteins these coupling constants are remarkably insensitive ($<\sim$0.2 Hz) to effects other than the dihedral angle. Proteins are relatively plastic molecules with little strain, no bad steric contacts, and in the case of ubiquitin, no highly charged atoms in the immediate vicinity of the polypeptide backbone. Our results therefore should not be interpreted to indicate that $^1H-^1H$ and $^1H-^{13}C$ *J* couplings are not sensitive to bond strain or strong electric field gradients.

As factors other than the intervening dihedral angle have only very small effects on the ^3J couplings related to ϕ, NMR offers the opportunity to determine the time-averaged ϕ angles in proteins with very high precision. For small proteins with short rotational correlation times, τ_c, the ultimate accuracy at which these angles can be determined by the NMR data rivals those of the highest resolution protein X-ray structures.

Acknowledgment. We thank Frank Delaglio and Dan Garrett for developing the software used to process and analyze the NMR data, Stephan Grzesiek, Nico Tjandra, John Marquardt, Marius Clore, Angela Gronenborn, and Dennis Torchia for stimulating discussions, Rolf Tschudin for building the gradient pulse-shaping unit and amplifier used in this study, and Sean Parkin for providing a preprint of reference 59. This work was supported by the AIDS Targeted Anti-Viral Program of the

(62) Braatz, J. A.; Paulsen, M. D.; Ornstein, R. L. *J. Biomol. Struct. Dyn.* **1992**, *9*, 935−949.

Office of the Director of the National Institutes of Health. A.C.W. is supported by an American Cancer Society post-doctoral fellowship (PF-4030).

Supporting Information Available: One table containing selective H^{α} relaxation rates; one table containing $^{3}J_{H^{N}H^{\alpha}}$, $^{3}J_{H^{N}C'}$, $^{3}J_{H^{N}C^{\beta}}$ and $^{3}J_{H^{\alpha}C'}$ coupling constants together with the backbone ϕ angles derived from the X-ray structure, the NMR data, and their combined use; one table containing the measured $^{3}J_{H^{N}H^{\alpha}}$ values measured using E.COSY, HNHA, and CT-HMQC techniques; one table containing the Δ_{ai} corrections; Bruker AMX pulse sequence code for the HNCA[HA]-E.COSY, HNCA[CB]-E.COSY, HNCA[C′]-E.COSY, and HCAN[C′]-E.COSY experiments and Bruker DMX code for the HN(CO)-HB experiment; ten figures, showing graphical representations of the pulse schemes; simulated multiplets showing the effects of $^{1}H^{\alpha}$ spin flips on the measured $^{3}J_{H^{N}H^{\alpha}}$; the relation between $^{3}J_{H^{N}H^{\alpha}}$ derived from CT-HMQC and $T_{1\alpha}$; plots of $^{2}J_{H^{\alpha}C'}$ from 2D-HSQC E.COSY *versus* those from 3D HN(CO)HB; plots of the deviation between measured J values, J_{meas}, and those predicted by the Karplus curve, J_{pred}, for $^{3}J_{H^{\alpha}C'}$ and $^{3}J_{H^{N}C^{\beta}}$; a plot of the correlation coefficient, r, between $J_{meas} - J_{pred}$ for $^{3}J_{H^{\alpha}C'}$ and $^{3}J_{H^{N}H^{\alpha}}$ (37 pages). This material is contained in many libraries on microfiche, immediately follows this article in the microfilm edition of the journal, can be ordered from the ACS, and can be downloaded from the Internet; see any current masthead page for ordering information and Internet access instructions.

JA9535524